Pioneering Advances in Materials

Journal homepage: http://piadm.sbu.ac.ir　　　

Shahid Beheshti University

Research paper

Innovative Plasmonic Coherence Tomography Using Nanomaterials: A Paradigm Shift in Imaging

Amir Reza Sadrolhosseini[1,2], Katayoon Samavati[1]* ORCID

[1]Department of Physics, NT.C. Islamic Azad University, Tehran, Iran

[2]Institute of Biosocial and Quantum Science and Technology, CT.C. Islamic Azad University, Tehran, Iran

*ksamavati@iau.ir

Abstract

Optical coherence tomography (OCT) is a high-potential and important technique for diagnosing diseases in ophthalmology, dermatology, dentistry, and gastroenterology. OCT has the potential to recognize the morphology and configuration of living tissues. Some medical methods such as X-rays have side effects, and they cannot be used repeatedly for diagnosing in dermatology and ophthalmology. OCT has the potential to investigate the layers of skin and retina. Therefore, OCT has been considered for diagnosing eye, skin, and dental diseases. Some analytical methods and nanomaterials have been suggested for increasing the sensitivity and resolution of OCT. Recently, some researchers have used quantum dots and plasmonic nanomaterials to enhance the quality and sensitivity of OCT images. Therefore, in this review, the significant parameters, and the important parts of the theory for optical coherence tomography have been presented with the plasmonic properties of nanoparticles. The famous methods for preparing plasmonic nanomaterials and their role have been discussed.

1. Introduction

Optical coherence tomography (OCT) is a versatile technique to observe the micrometer variation in the thickness of human tissue and the main application of OCT is in ophthalmology for retinal imaging, in cardiology for intravascular imaging, and dermatology [1]. The improvement of resolution, response time, and accuracy is an intensely interesting matter for the development of the OCT technique [2]. The history of OCT dates back to the early 1990s when it was first developed as a non-invasive imaging modality for biological tissues. In 1991, James G. Fujimoto, Eric A. Swanson, and David Huang [3], working at the Massachusetts Institute of Technology (MIT), introduced the concept of Optical Coherence Tomography. Their groundbreaking work was published in the journal Science, detailing the principles of OCT

and demonstrating its potential for high-resolution imaging of biological tissues [3]. The early OCT systems utilized low-coherence interferometry to capture cross-sectional images of tissues with micrometer-scale resolution. These systems employed a Michelson interferometer setup with a broadband light source, such as a super-luminescent diode, to generate interference patterns. This approach allowed for the measurement of the echo time delay of backscattered light, enabling the reconstruction of tissue microstructure [4]. In the late 1990s and early 2000s [5], OCT technology advanced rapidly, leading to significant improvements in imaging speed, resolution, and depth penetration. Researchers and engineers developed Fourier-domain OCT (FD-OCT) techniques, such as spectral-domain OCT (SD-OCT) and swept-source OCT (SS-OCT). These approaches replaced time-domain detection with spectrally resolved detection, enhancing imaging performance and enabling real-time imaging capabilities. OCT has found widespread application in ophthalmology for diagnosing and monitoring various retinal diseases, including age-related macular degeneration, diabetic retinopathy, and glaucoma. The ability of OCT to visualize retinal layers and detect pathological changes revolutionized the field of ophthalmic imaging, leading to improved patient care and outcomes [6]. In addition to ophthalmology, OCT has been extensively applied in cardiology for intravascular imaging of coronary arteries. Intravascular OCT (IVOCT) provides high-resolution cross-sectional images of coronary artery walls, allowing for the visualization of atherosclerotic plaques and guiding interventional procedures such as stent placement. The use of IVOCT has significantly improved the assessment of coronary artery disease and optimized treatment strategies [7]. In recent years, OCT has continued to evolve with advancements in imaging technology, signal processing algorithms, and clinical applications. The ongoing development of next-generation OCT systems promises further improvements in imaging speed, resolution, and functionality, paving the way for enhanced diagnosis, monitoring, and treatment guidance across various medical specialties [8].

There are many methods that have been used to improve the OCT technique to obtain a high-quality image. Among the methods, such as enhanced light sources [5], Fourier-domain OCT (FD-OCT) [8], adaptive optics [9], signal processing algorithms [4], and motion correction techniques [10] are significant, and the OCT commercial machines were developed based on the mentioned techniques. Another technique to improve the performance of the OCT technique is based on the plasmonic properties of nanomaterials [11].

The plasmonic properties of nanostructures discuss the interaction of light beams with free electrons in the metallic or conductive nanostructure to excite the plasmonic wave at the interface of two media with opposite dielectric signs [12]. Therefore, the plasmonic properties of nanomaterials can enhance the contrast of OCT, increase the sensitivity and selectivity of OCT, and plasmonic is a theragnostic agent [11]. Recently, the combination of plasmonic with optical coherence tomography is an innovative approach to improve the sensitivity, resolution, response time, and application of images. The exploit of plasmonic properties of nanomaterials and OCT is a unique and powerful imaging technique for its high resolution and non-invasive nature [13].

Plasmonic properties offer several advantages in image devices due to their ability to manipulate light at the nanoscale. The considerable advances include enhanced light-matter interaction [14], subwavelength resolution [15, 16], tunability [14], surface sensing and imaging [17], compactness and integration [14], and real-time imaging [14] in the medical and industrial image systems.

OCT technique is a powerful imaging method with several capabilities including high-resolution imaging [4], non-invasive imaging [5], real-time imaging [5], depth profiling [4], high-speed imaging [5], and multimodal imaging integration [3]. Therefore, the OCT technique is a useful imaging method in the medical image field and it offers a versatile and powerful imaging tool for a wide range of biomedical applications, including diagnostics, monitoring disease progression, and guiding therapeutic interventions the main reasons to combine the OCT technique with plasmonic technology is enhanced contrast and sensitivity [18], improved depth resolution [19], functional imaging [20], and multimodal imaging [21].

The nanomaterials have more applications in medicine including biosensors, measurement the

chemical and biochemical molecules [22, 23], temperature [24], and enhancement of the fluorescent emission [25, 26]. The significant nanoparticles and nanostructures that have been utilized to improve the OCT techniques including gold nanoparticles (Au-NPs) [27], silver nanoparticles (Ag-NPs) [28], silica nanoparticles [20], gold nano-star [29], gold nano-rod [30], gold nano-plats [31] , copper sulfide nanoparticles (CuS-NPs) [32], carbon nanotubes (CNTs) [33] , and quantum dots (QDs) (cadmium selenide, indium phosphide, lead sulfide, indium arsenide, and, cadmium telluride) [34]. The mentioned nanostructure holds promises for improving OCT imaging by providing enhanced contrast, sensitivity, and molecular specificity for various biomedical applications.

A pivotal and innovative feature of this review is the investigation of the plasmonic effect within the framework of OCT. By utilizing the synergistic strengths of these two methods, researchers have achieved remarkable advancements in imaging, resulting in improvements in contrast, sensitivity, and depth resolution. This review delves into the fundamentals of Optical Coherence Tomography (OCT), the associated challenges and limitations of OCT, the essential mechanisms of the plasmonic technique, and the characteristics of the aforementioned nanoparticles and nanostructures, elaborating on the generation and manipulation of surface plasmons to realize exceptional imaging capabilities.

2. Basic of Optical Coherence Tomography and Plasmonic

2.1 Main idea for OCT
OCT is frequently likened to medical ultrasound due to its analogous operational principles. Both methods of medical imaging utilize waves to capture the image and direct waves toward the tissue being examined, where these waves bounce off the tissue's structure. Subsequently, the waves that reflect are scrutinized, and their time delay is gauged to ascertain the depth at which the reflection took place. However, OCT utilizes light in the near-infrared spectrum, which travels considerably faster than ultrasound waves. Consequently, it's not feasible to directly

measure the delays of the waves reflecting. Hence, a reference measurement is employed and it is achieved through an interferometer, wherein a portion of the light is directed toward the sample, while another fraction is routed to a reference arm with a precisely known length [35].

The fundamental concept behind all implementations of OCT is based on low-coherence interferometry. Temporal coherence refers to a light source's property, describing the continuity of its wave train over time at a specific spatial point. When a light source emits wave trains with low temporal coherence, their phase relationship remains consistent only for a brief duration, known as the coherence length or coherence gate. A light source with a broad spectral bandwidth comprises various wavelengths, resulting in low coherence, whereas monochromatic laser light, with its narrow spectral line, maintains coherence over longer distances, typically several meters.

In an interferometer setup, light from the source is divided into two paths and then recombined at the output. This recombination allows for interference under specific conditions: coherent waves either reinforce each other (constructive interference) or cancel each other out (destructive interference), or exhibit any level of interference in between. The resulting light intensity is detected as an electrical signal by a photodetector. This signal is dependent on the difference in optical path lengths between the two arms of the interferometer [36].

For a light source with low coherence, such as a super-luminescent diode (SLD) or a pulsed laser source, interference can only occur if the optical paths are closely matched in length within the short coherence length of the source, typically on the order of micrometers.

2.2 Theory of OCT (Time and Fourier domains)
Figure 1 shows the Michelson setup that is used to capture the image in the OCT. The monochromatic light source can be used for interference with the two light beams in the interferometer. Generally, the Michelson interferometer contains two mirrors (one mirror is a reference and the second mirror is a sample), a beam splitter, and a detector.

In OCT, coherence length is a critical parameter that defines the depth resolution of the imaging system. It represents the maximum optical path

difference between the reference and sample arms of the interferometer at which interference fringes can still be observed, thereby indicating the depth range over which the system can produce high-resolution images. The coherence length in OCT is the distance over which a light source maintains a specified degree of coherence, which is crucial for producing clear interference patterns. It determines the axial resolution of the OCT system, with a shorter coherence length corresponding to a higher resolution. The coherence length can be mathematically expressed as [8]:

$$L_c = \frac{4\ln 2}{\pi} \times \frac{\lambda_0^2}{\Delta\lambda} \qquad (1)$$

Where λ_0 and $\Delta\lambda$ are the central wavelength of the light source and the full width at half maximum (FWHM) of the source's spectral bandwidth, respectively.

This formula shows that the coherence length is inversely proportional to the spectral bandwidth; hence, a broader bandwidth results in a shorter coherence length and higher axial resolution [8]. The coherence length is related to coherence time as follows:

$$L_c = c\tau_c \qquad (2)$$

In practical terms, OCT systems use light sources with broad bandwidths, such as SLD or femtosecond lasers, to achieve the short coherence lengths needed for high-resolution imaging (QLI).

This allows OCT to produce detailed images of internal tissue structures with micrometer-level resolution, making it a powerful tool for medical imaging, particularly in ophthalmology.

OCT is based on Michelson interferometry, and the low-coherence light source should be used to capture the image.

There are two generations of OCT to acquire the high-resolution image, including time-domain OCT (TD-OCT) and Fourier-domain OCT (FD-OCT).

Figures 1a and 1b show the OCT setup based on Michelson interferometry.

When the light beam (reference part) was reflected from the reference mirror, another beam, as a biological beam, was backscattered from various layers in the biological sample, such as tissue or retina.
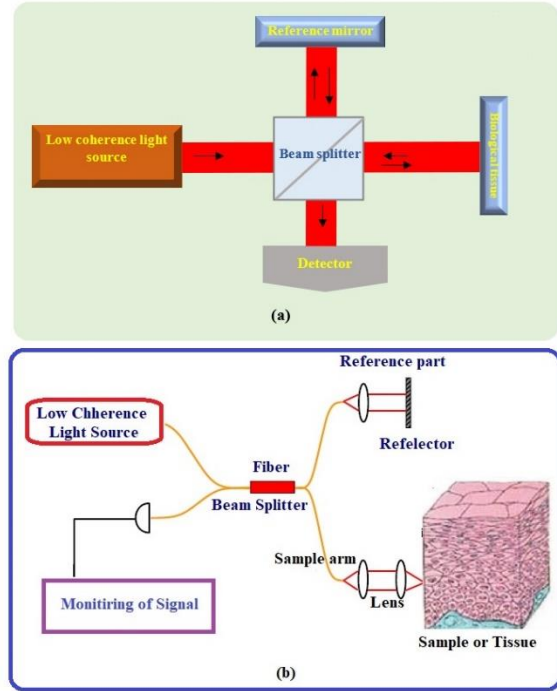

Figure 1. The Michelson interferometer scheme for the investigation of OCT a) free space diagram, b) Fiber optics diagram.

Time-domain optical coherence tomography (TD-OCT) is an imaging technique used to obtain high-resolution cross-sectional images of biological tissues. TD-OCT uses a light source with a short coherence length to produce a broad spectrum of light [36]. The system typically uses a Michelson interferometer setup (Figure 1), which splits the light into two arms, including a reference arm and a sample arm. In the reference arm, the light is directed to a mirror, and this mirror is mounted on a scanning mechanism to change its position, allowing the length of the reference arm to be varied. In the sample arm or biological arm, the light is directed onto the tissue or retina being imaged. The light penetrates the tissue or retina and is backscattered from different depths or layers within the sample, and the reflected light from the sample is recombined with the reflected light from the reference mirror. Due to the coherence properties of the light, interference occurs only when the optical path lengths of the two arms match the coherence length of the light source. The interference signal is detected by a photodetector. By moving the reference mirror, the path length is varied, and the detector records

the intensity of the interference signal as a function of the reference mirror position. The reference mirror's movement modulates the interference signal over time, creating a depth profile (A-scan) of the sample [37]. Therefore, a two-dimensional cross-sectional image (B-scan) is generated by scanning the sample beam laterally across the tissue and acquiring multiple A-scans. The detected signals are processed to reconstruct the image, providing detailed information about the tissue's microstructure. This process allows TD-OCT to provide real-time, non-invasive imaging of tissue structures at a micrometer resolution [38].

The axial resolution in time-domain optical coherence tomography (TD-OCT) is a crucial factor that determines the system's capability to differentiate between two points along the depth direction within a sample. This resolution is governed by the coherence length of the light source used. The coherence length, explained by Equation 1, is the distance over which the light waves remain in phase and is inversely related to the light source's bandwidth ($\Delta\lambda$). Therefore, the axial resolution (Δz_R) in TD-OCT is directly proportional to the coherence length, and the axial resolution in air is defined accordingly.

$$\Delta z_R = \frac{L_c}{2} \tag{3}$$

Consequently, the axial resolution can be derived as follows:

$$\Delta z_R = \frac{2\ln 2}{\pi} \times \frac{\lambda_0^2}{\Delta\lambda} \tag{4}$$

The axial resolution within biological tissue is obtained by dividing the axial resolution in air by the tissue's refractive index [39].

Eq. (4) shows that the axial resolution improves with a broader bandwidth ($\Delta\lambda$) of the light source and is centered around the wavelength (λ_0) used. In TD-OCT, light from a broadband source is split into a sample arm and a reference arm. The interference pattern is produced when the optical path lengths match within the coherence length. By moving the reference mirror and detecting the interference signal, the system can determine the depth information of the sample. The varying position of the reference mirror modulates the interference signal, enabling the acquisition of depth profiles (A-

scans) [36, 39]. The coherence length dictates the precision of these depth measurements.

The transverse resolution of OCT is defined as the focal diameter of the incident sample beam, which is independent of the coherence length of the source. If the transverse distribution of the incident sample beam is Gaussian, the transverse resolution is given by

$$\Delta r_R = \frac{4\lambda_0}{\pi} \times \frac{f}{D} \tag{5}$$

Where f and D are the focal length of the objective and the diameter of the beam on the lens. The numerical aperture equals the ratio of the diameter of the beam or lens to twice of focal length. Therefore, the transverse resolution or lateral resolution is as follows [36, 39]:

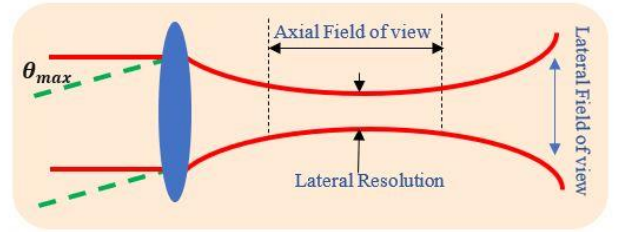$$\Delta r_R = \frac{2\lambda_0}{\pi} \times \frac{1}{NA} \tag{6}$$

Figure 2. Diagram of OCT at the sample beam to show the resolution parameters and field of view.

The depth range within which the lateral resolution is approximately maintained is defined by the depth of focus Δz_f as follows:

$$\Delta z_f = \frac{\pi \Delta r_R^2}{2\lambda_0} \tag{7}$$

The depth of focus is equal to twice the Rayleigh range of the Gaussian beam. Eq. (7) illustrates the balance between the focal diameter and the focal zone of the sample beam, which is narrower and shorter than the focal beam diameter and focal zone, respectively. Consequently, employing a high numerical aperture objective lens necessitates either transverse-priority scanning, as seen in enface imaging (c-scan), or depth-priority scanning with dynamic focusing along the optical axis [40].

The axial field of view (FOV_{axial}) in OCT (Figure 2) refers to the depth range that can be imaged. Typically, in OCT systems, this axial range is around 2-3 millimeters in tissue. The specific value can vary based on the particular OCT system and its configuration, but this depth is commonly sufficient for most clinical applications, such as retinal imaging, where detailed cross-sectional views of tissue layers are required [35]. The FOV_{axial} deepened on wavelength as follows:

$$FOV_{axial} = \frac{0.565\lambda}{\sin^{-1}\left[\frac{\sin^{-1}(NA)}{2}\right]} \qquad (8)$$

The lateral field of view ($FOV_{lateral}$) in OCT (Figure 2) refers to the width or area that can be imaged across the sample surface. This lateral FOV is typically limited in standard OCT systems but can be expanded with advanced techniques [41]. The $FOV_{lateral}$ is proportional to the focal length as follows:

$$FOV_{lateral} = 2f\theta_{max} \qquad (9)$$

Fourier domain optical coherence tomography (FD-OCT) is an advanced imaging technology that provides high-resolution cross-sectional images of tissues. It offers several advantages over traditional time-domain OCT, primarily due to its use of spectral interferometry and Fourier transformation. The benefits of FD-OCT are as follows:

High-Speed Imaging: FD-OCT can acquire images much faster than time-domain OCT. This is due to its ability to simultaneously capture depth information across the entire sample using a spectrometer and a fixed reference arm [42].

Enhanced Sensitivity: FD-OCT improves sensitivity, allowing for better image quality and resolution. This is particularly useful in medical diagnostics, where detailed visualization of tissue microstructures is crucial [43].

Ultrahigh Resolution: FD-OCT can achieve ultrahigh resolution, on the order of a few micrometers, making it ideal for detailed imaging of biological tissues such as the retina [44].

This technology is widely used in ophthalmology for retinal imaging, helping in the diagnosis and management of diseases like glaucoma and macular degeneration. It is also used in other fields for imaging various tissues and structures [42]. FD-OCT leverages the principles of spectral interferometry, where light from the reference and sample arms is spectrally separated, detected, and then converted into depth information using the Fourier transformation [45-47].

Figure 3 demonstrates the Fourier-domain OCT system, which relies on spectral interferometry. FD-OCT depends on the Fourier transformation of the interference signal for extracting depth-specific data from a specimen. The spectral interferogram can be obtained by expressing the spectral components of the sample (tissue) and reference beams in the following manner [54]:

$$E_R(\omega) = E_0(\omega)r_R\exp\left[i(2k_R(\omega)l_R - \omega t\right) \qquad (10)$$

$$E_S(\omega) = E_0(\omega) \int_{-\infty}^{+\infty} \acute{r}_S(l_S) \exp[i(2k_S(\omega)l_S - \omega t)]\, dl_S \qquad (11)$$

Where E_0, r_R, and $\acute{r}_S(l_S)$ are the initial electrical field amplitude of the reflected beam from the reference reflector, and the amplitude of the reflected beam from the sample (tissue). $\acute{r}_S(l_S)$ expresses the image and it is the backscatter from the sample. The initial light beam may be scattered on the surface of samples (tissue), as a result, the attenuation has occurred and the amplitude has decreased. Therefore, $\acute{r}_S(l_S)$ is the reflectivity density and it can be obtained from the amplitude of the reflected beam (r_S) using the Dirac delta function as follows:

$$\acute{r}_S(l_S) = r_S(l_{S0})\delta(l_S - l_{S0}) \qquad (12)$$

Where l_{S0} is the location of the mirror. $r_S(l_{S0})$ can be ameliorated, if $\acute{r}_S(l_S)$ can be defined integer value near the l_{S0}. The medium is free dispersion, so the refractive index is unity in the reference part, and k_R is proportional to $\frac{\omega}{c}$. The refractive index of the sample (tissue) is n_S and the ratio of $\frac{k_S}{n_S}$ is equivalent to $\frac{\omega}{c}$. Therefore, the spectral interferogram of OCT can be rewritten as follows:

$$I(k) = |E_R(kc) + E_S(kc)|^2 \qquad (13)$$

So, the spectral interferogram can be expressed by using Eqs. (10) and (11) as follows [48][54]:

$$I(k) = S(k)r_R^2 +$$
$$2S(k)r_R \int_{-\infty}^{+\infty} \acute{r}_S(l_S) Cos\big(2k(n_S l_S - l_R)\big) dl_S$$
$$+S(k)\left|\int_{-\infty}^{+\infty} \acute{r}_S(l_S) \exp\big(i2k(n_S l_S)\big) dl_S\right|^2 \quad (14)$$

$I(k)$ is the main formula to explain the OCT spectra, and it is related to the source power via the density distribution $(S(k))$. Eq. (14) has three terms. The first term corresponds to the reference intensity, and it can be measured by fixing the sample(tissue) when the $\acute{r}_S(l_S)$ Zero. The second term assigns the cross-interference. The third term expresses the self-interference was driven by the power spectra including $|E_S(c)|^2$. The self-interference term refers to interference waves from the different parts of the sample. The important part is the cross-interference term because it can be decoded to extract $\acute{r}_S(l_S)$ by taking the inverse Fourier transformation.

To find the true image, the reference point can be shifted to the image reference reflector point at the sample point area ($l_R = 0$).

In this case, the even function $(\widehat{r}_S)$ can be replaced by $\acute{r}_S$ .When the variable of integration is changed to $l_S = \acute{l}_S/2n_S$ and Dirac delta function is $\delta(\acute{l}_S) = \frac{1}{n_S}\delta(\frac{l_S}{2n_S})$. Another interferogram can be derived from Eq. (14) by using the Fourier transform, convolution, and autocorrelation function as follows [8]:

$$I_2(k) = S(k)\left\{r_R^2 - \frac{r_R}{2n_S}\mathfrak{F}\left\{\widehat{r}_S(\frac{l_S}{2n_S})\right\}(k) + \frac{1}{16n_S^2}\left|\mathfrak{F}\left\{\widehat{r}_S\left(\frac{\acute{l}_S}{2n_S}\right)\right\}(k)\right|^2\right\} \quad (15)$$

And the difference between Eqs. (14) and (15) is

$$\Delta I(k) = I(k) - I_2(k) = S(k)\frac{r_R}{n_S}\mathfrak{F}\left\{\widehat{r}_S\left(\frac{l_S}{2n_S}\right)\right\}(k) \quad (16)$$

Therefore, the line image can be derived as follows:

$$\widehat{r}_S(l_S) = \frac{n_S}{r_R}\mathfrak{F}^{-1}\left\{\frac{\Delta I(k)}{S(k)}\right\}(2n_S l_S) \quad (17)$$

FD-OCT employs a mathematical equation to transform the interference signal into a depth profile using Eq. (17). A spectrometer produces a spectrum with uniformly distributed wavelengths that undergo a Fourier transformation algorithm. During the process of laser wavelength variation, a photodetector that is composed of only one element is utilized to measure the interference signal. A hardware device known as a "k-clock" can maintain consistent intervals. Theoretical analysis can be applied without alterations [45].
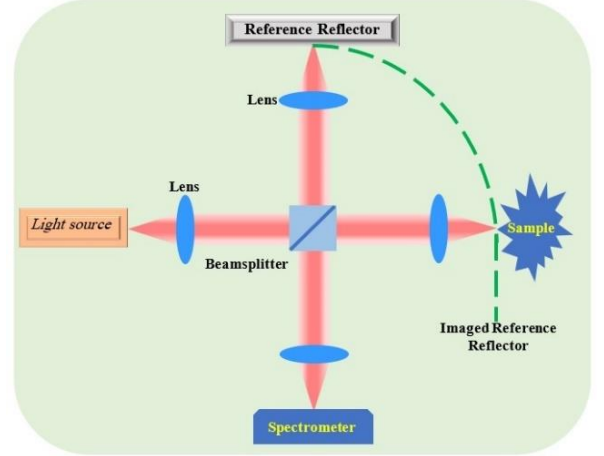

Figure 3. Michaelson interferometer for FD-OCT experiment.

2.3 Challenges and OCT limitations
As a previous section, the mechanism and configuration of OCT are based on Michelson interferometry, and two domains should be considered for analysis and data acquisition. Therefore, OCT technology faces challenges such as determining the most suitable device for clinical purposes, managing acquisition time, and scanning areas in wide-field OCT angiography [49], and addressing technical complexities in newer OCT technologies [50], and there are limitations of OCT, including limited penetration depth, motion artifacts due to patient movement, limited axial resolution, highly scattering tissues, and limited field of view.

2.3.1 Limited penetration depth hinders the visualization of deeper tissue layers
OCT faces limitations due to its limited penetration depth, hindering the visualization of deeper tissue layers. Typically restricted to 1 to 1.5 mm in turbid tissue, this depth is constrained by the confounding effects of optical scattering, particularly in biological tissues [51]. In most

biological tissues, the penetration depth is limited by scattering to a few millimeters, with scattering decreasing monotonically with increasing depth [2]. These limitations can impede the comprehensive examination of structures located deeper within tissues, posing challenges in diagnosing certain conditions and understanding tissue morphology.

2.3.2 Motion artifacts due to patient movement may distort images

Motion artifacts caused by patient movement during OCT imaging can distort images, leading to inaccuracies in diagnosis and assessment. These artifacts occur when the patient's eye moves during scanning, causing distortion or double scanning of the same area [2]. Eye movement can result in poor image quality, affecting the clarity and reliability of OCT scans. Longer image acquisition times may exacerbate this issue by increasing the likelihood of patient movement and reducing patient cooperation [52]. Correcting motion artifacts is crucial for obtaining accurate OCT images, and various techniques, such as motion artifact correction algorithms, have been developed to mitigate their effects [53]. Despite these efforts, motion artifacts remain a significant limitation in OCT imaging, particularly in cases where patient cooperation is challenging or when imaging mobile structures.

2.3.3 Limited axial resolution can affect the ability to distinguish fine structures

Limited axial resolution in OCT can indeed impact the ability to distinguish fine structures. Axial resolution is determined by the bandwidth of the light source used in OCT imaging. While ultrahigh-resolution OCT systems can achieve axial resolutions of around 3-5 μm, conventional OCT typically provides axial resolutions ranging from 10 to 20 μm [54]. This limitation can affect the visualization of fine details within tissues, particularly in structures with closely spaced features or in scenarios where precise morphological information is crucial. Despite advancements, such as polarization-sensitive OCT, which has the potential for higher spatial resolution, limitations in axial resolution persist, impacting the ability to resolve intricate tissue structures [55]. Therefore, while OCT provides remarkable imaging capabilities, its

effectiveness in resolving fine structures is contingent upon the system's axial.

2.3.4 Challenges in imaging highly scattering tissues like the retinal pigment epithelium

Imaging highly scattering tissues like the retinal pigment epithelium (RPE) poses challenges for OCT due to limited penetration depth and sensitivity to scattering. The RPE is located beneath the retina and has a high scattering coefficient, which can affect the quality of OCT images. This limitation arises because the high scattering properties of the RPE can obscure underlying structures and reduce image contrast [56]. Furthermore, traditional time-domain OCT (TD-OCT) systems face limitations in imaging highly scattering tissues efficiently due to their slow imaging speed [49]. Spectral-domain OCT (SD-OCT) systems offer improved imaging capabilities, including better visualization of the RPE layer, but challenges related to scattering and contrast persist [56]. Overcoming these challenges involves advancements in OCT technology, such as optimization of light sources and signal processing techniques to enhance imaging performance in highly scattering tissues like the RPE.

2.3.5 Limited field of view, particularly in traditional OCT systems

Limited field of view is a notable limitation, especially in traditional OCT systems. These systems often have a restricted imaging range, which can make it challenging to capture comprehensive images of larger structures or areas of interest. This limitation is particularly relevant in ophthalmology, where imaging the entire retina or optic nerve head may require multiple scans and stitching together of images [57]. Moreover, traditional OCT systems may struggle to visualize structures beyond the central field of view without the need for manual adjustment or multiple acquisitions, leading to potential gaps in the imaging data [58].

3. Plasmonic and Role of Nanostructure

3.1. Principals of Plasmonic

Plasmonic and surface plasmon reverberation innovations have discovered assorted applications in detecting, identifying, and recognizing biomolecules [59] and chemical

compounds. Understanding plasmonic, counting concepts like plasmon, plasma recurrence, and surface plasmon reverberation (SPR), is pivotal for illustrating how light interatomic with nanoscale materials, especially metal nanoparticles. For example, the plasma recurrence, inferred from the Drude demonstration, makes a difference in evaluating the straightforwardness of materials and inexact their dielectric function, subsequently empowering the finding of light behavior in metals and dielectrics.

Surface plasmon reverberation (SPR) is an optical marvel happening at the interface between a metal and a dielectric medium, driven by charge thickness vacillations. Metal nanoparticles show SPR and plasmonic properties over the unmistakable and near-infrared electromagnetic range. Localized surface plasmon reverberation (LSPR) happens at the surfaces of metallic nanoparticles and their encompassing medium, characterized by short-length scales. The recurrence and escalation of LSPR are affected by nanoparticle size and morphology. Computational strategies like finite-difference time-domain (FDTD) and limited component strategy (FEM) are commonly utilized to unravel differential conditions and analyze SPR, LSPR, and SPRi yield. Surface plasmon reverberation (SPR) is accomplished through photon-induced swaying of charges in small gold or silver particles and finds broad applications in different areas, including fabric science, science, pharmacology, and nanoelectronics.

Method of coupling (Prism, grating, and waveguide), moreover known as the Kretschmann arrangement (Figure 4), includes the utilization of a high-index optical element such as a prism with a lean layer of metal such as gold or silver coated on its surface. A monochromatic light bar, such as a ruddy laser, is coordinated through the high-index prism. Upon coming to the metal layer, a parcel of the light is reflected whereas another parcel gets to be an inhomogeneous wave engendering inside the gold or silver layer. This proliferating portion is known as the transitory wave, which exponentially rots inside the metal layer, with the profundity of entrance subordinate to both the metal layer thickness and the vitality of the light bar.
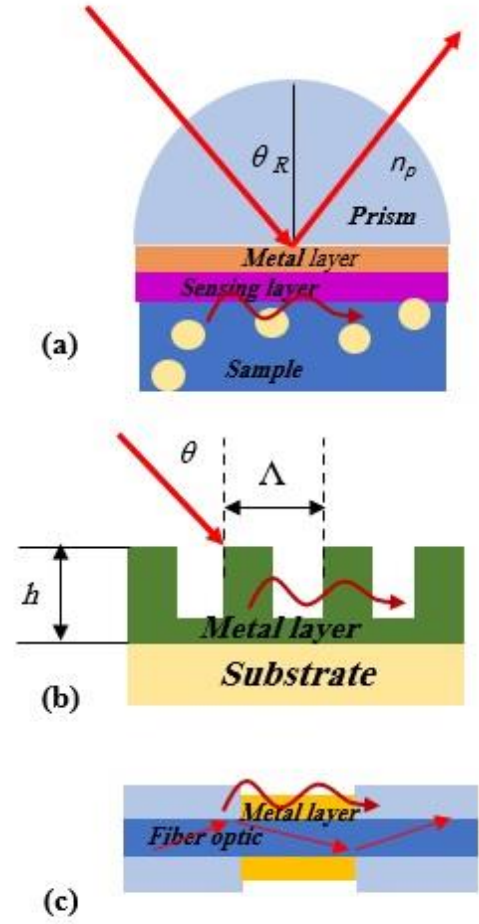

Figure 4. a) prism coupling, b) grating coupling, and c) waveguide coupling [58].

Figure 4a shows the prism coupling configuration and the optical parameters including n_p, ε_m, ε_d, and θ_R are the refractive index of the prism, the dielectric constant of the gold or silver layer, the dielectric constant of the dielectric layer, and the angle of resonance, respectively. The resonance condition can be expressed as follows:

$$n_p \sin \theta_R = \mathrm{Re}\left(k \sqrt{\frac{\varepsilon_d \varepsilon_m}{\varepsilon_d + \varepsilon_m}} \right) = n_{sp,ef}$$

(18)

where ε_{mr} and ε_{mi} are the real and imaginary components of the metal layer. Therefore, the effective index and the attenuation constant (b)

can be expressed as follows [60, 61]:

$$n_{ef} = \frac{c}{\omega} \mathrm{Re}\left(k\sqrt{\frac{\varepsilon_d \varepsilon_m}{\varepsilon_d + \varepsilon_m}} \right)$$
(19)

$$b = 0.087 \, \mathrm{Im}\left(k\sqrt{\frac{\varepsilon_d \varepsilon_m}{\varepsilon_d + \varepsilon_m}} \right)$$
(20)

The attenuation b is expressed in units of dB cm^{-1}. When the light beam passes through the prism, I_i, and I_r , respectively denote the initial amplitude of the light beam and the amplitude of the reflected light beam after interacting with the metal layer. According to Fresnel's theory, the amplitude of the reflected light beam can be described as follows [60]:

$$I_r = I_i \times e^{i\phi} r_{pmd}$$
(21)

r_{pmd} represents the reflection coefficient of the light beam from the metal-dielectric interface within the prism, and its expression is as follows [60, 62]:

$$r_{pmd} = \frac{r_{pm} + r_{md} e^{(2ik_{mx}q)}}{r_{pm} + r_{pm} r_{md} e^{(2ik_{mx}q)}}$$
(22)

The variables r_{pm}, r_{md}, and k_{mx} represent the amplitude of the reflection coefficient from the prism-metal interface, the amplitude of the reflection coefficient from the metal-dielectric medium positioned after the gold or silver layer, and the propagation constant, respectively. The reflection coefficient for the TM mode of a light beam and the propagation constant are expressed as follows:

$$r_{pm} = \frac{\varepsilon_m k_{px} - \varepsilon_p k_{mx}}{\varepsilon_m k_{px} + \varepsilon_p k_{mx}}$$
(23)

$$r_{md} = \frac{\varepsilon_d k_{mx} - \varepsilon_m k_{dx}}{\varepsilon_d k_{mx} + \varepsilon_m k_{dx}}$$
(24)

$$k_{mx} = \sqrt{\left(\frac{2\pi}{\lambda}\right)^2 \varepsilon_m - \left(\frac{2\pi}{\lambda}\right) n_p \sin\theta}$$
(25)

$$k_{px} = \sqrt{\left(\frac{2\pi}{\lambda}\right)^2 \varepsilon_p - \left(\frac{2\pi}{\lambda}\right) n_p \sin\theta}$$
(26)

$$k_{dx} = \sqrt{\left(\frac{2\pi}{\lambda}\right)^2 \varepsilon_d - \left(\frac{2\pi}{\lambda}\right) n_p \sin\theta}$$
(27)

As a result, the reflectance (R) can be calculated as the square of the reflection coefficient, as shown below:

$$R = \left| r_{pmd} \right|^2$$
(28)

Equation (28) can be utilized for modeling the SPR signal. The amplitude of the reflectivity (R) varies with the angle and refractive index. Therefore, by comparing the experimental reflectance values with the theoretical ones, obtained through the minimum root square, the refractive index and resonance angle shift can be determined.

$$T = \sum \left[R_{th}(\theta, n) - R_{Ex}(\theta, n) \right]$$
(29)

In the prism coupling method, the attenuation of the light beam is a crucial parameter in sensor design. This attenuation is proportional to the length (ℓ) of surface plasmon decay, as outlined below [63]:

$$\ell = \left[\frac{\varepsilon_{mi}}{(\varepsilon_{mr})^2} \times \frac{\omega}{2c} \times \left(\frac{\varepsilon_{mr} \varepsilon_d}{\varepsilon_{mr} + \varepsilon_d} \right)^{(3/2)} \right]^{-1}$$
(30)

3.2 Localized Surface Plasmon Resonance
Localized surface plasmon resonance (LSPR) is a phenomenon that occurs when metal nanoparticles, typically gold or silver, exhibit strong absorption and scattering of light due to the collective oscillation of their conduction electrons. This resonance phenomenon is highly dependent on the size, shape, and composition of the nanoparticles. The resonance wavelength of LSPR can be described by the Mie theory, which takes into account parameters such as the size and refractive index of the nanoparticles. The intensity and wavelength of the LSPR peak are influenced by factors such as nanoparticle

morphology and the surrounding environment. LSPR has diverse applications in sensing, imaging, and photothermal therapy, making it a valuable tool in nanotechnology and biomedical research. For instance, in biosensing applications, changes in the LSPR peak position or intensity can be correlated with analyte binding events, enabling sensitive detection of biomolecules. The resonance wavelength of LSPR can be approximated using the Mie theory, which relates the resonance wavelength (λ) to the size (d) and refractive index (n) of the nanoparticles [64]:

$$\lambda = 2\pi d \sqrt{\frac{n^2-1}{n^2+2}} \qquad (31)$$

LSPR plays a crucial role in OCT due to its ability to enhance the quality of imaging. LSPR occurs when metal nanoparticles, such as gold or silver, resonate with incident light, resulting in strong absorption and scattering. In OCT, LSPR nanoparticles can be used as contrast agents to improve the imaging of biological tissues. The enhancement in contrast provided by LSPR enables better visualization of tissue structures and pathological features, leading to improved diagnostic accuracy. Additionally, LSPR nanoparticles can be functionalized to target specific biomolecules or cellular structures, enabling molecular imaging in OCT [65]. LSPR has been utilized to improve several parameters in OCT, including [65] contrast, sensitivity, and targeted image.

LSPR nanoparticles serve as contrast agents in OCT, enhancing the contrast between different tissue structures. By selectively binding to specific biomolecules or cellular targets, LSPR nanoparticles can highlight pathological features or regions of interest within biological tissues, improving image contrast.

The presence of LSPR nanoparticles increases the sensitivity of OCT imaging, allowing for the detection of subtle changes or abnormalities in tissue morphology. This enhanced sensitivity enables more accurate diagnosis and monitoring of diseases.

Functionalization of LSPR nanoparticles enables targeted imaging in OCT. By conjugating targeting ligands or biomolecules onto the nanoparticle surface, specific cellular or molecular targets can be identified and visualized with high specificity, providing valuable information for biomedical research and clinical diagnosis.

3.3 Gold Nanoparticles and Nanoplates

Gold nanoparticles (Au-NPs) hold significant potential to enhance OCT imaging. Their unique optical properties, including strong light scattering and absorption characteristics, make them promising contrast agents for improving the sensitivity and specificity of OCT imaging. Au-NPs have particular plasmonic properties, and they have a spherical shape and LSPR peak around 530 nm (Figure 5a). Moreover, Au-NPs can be utilized as contrast agents for enhancing OCT imaging of biological tissues [66]. In this case, Au-NPs can significantly enhance the backscattering signal of OCT images, leading to improved visualization of tissue microstructures. This enhancement allows for better delineation of tissue boundaries and detection of pathological changes at the cellular and subcellular levels.

Additionally, Au-NPs can be functionalized by targeting ligands or biomolecules to specifically accumulate in diseased tissues, further improving the diagnostic accuracy of OCT imaging. For example, Au-NPs were used as a target [67] for molecular imaging of cancer cells, demonstrating their potential for precise detection and characterization of tumor tissues using OCT [67]. Consequently, Au-NPs offer several advantages, including enhanced contrast, targeted imaging, biocompatibility, tunable optical properties, stability, and multimodal imaging for OCT imaging, and each one has been briefly explained as follows:

3.3.1 Enhanced Contrast: Au-NPs exhibit strong light scattering and absorption properties, enhancing the contrast in OCT images and improving visualization of tissue microstructures.

3.3.2 Targeted Imaging: Au-NPs can be functionalized with targeting ligands or biomolecules, allowing for targeted imaging of specific cells or tissues, which enhances diagnostic accuracy and reduces false positives.

3.3.3 Biocompatibility: Gold is inherently biocompatible, making Au-NPs suitable for biomedical applications such as OCT imaging.

Their low toxicity and minimal immune response make them ideal contrast agents for in vivo imaging.

3.3.4 Tunable Optical Properties: The optical properties of Au-NPs can be precisely controlled by adjusting their size, shape, and surface chemistry, allowing for tailored contrast enhancement in OCT imaging.

3.3.5 Stability: Au-NPs exhibit excellent stability in biological environments, ensuring long-term performance as contrast agents for OCT imaging without degradation or aggregation.

3.3.6 Multimodal Imaging: Au-NPs can be used in combination with other imaging modalities such as photoacoustic imaging or fluorescence imaging, enabling multimodal imaging approaches for comprehensive tissue characterization.

Overall, the use of Au-NPs as contrast agents in OCT imaging holds promise for advancing diagnostic capabilities in various biomedical applications, including ophthalmology, cardiology, and oncology. Au-NPs have demonstrated potential as contrast agents for some medical images, such as optical coherence tomography, for obtaining the image from retina or tumors.

However, their practical application in medicine is restricted because their peak wavelength coincides with that of hemoglobin, reducing their effectiveness.

To tackle this issue, researchers have explored Au-NPs that absorb near-infrared (NIR) light since biological tissues have lower NIR absorption rates. Different shapes of Au-NPs, including spheres, rods, stars, shells, and thin plates, have been investigated as NIR contrast agents for OCT imaging, enhancing molecular imaging capabilities. Nevertheless, many of these Au-NPs are produced using cetyltrimethylammonium bromide (CTAB), which poses risks of long-term toxicity and often tends to be larger. For effective in vivo medical imaging, Au-NPs should ideally be smaller than 100 nm. Furthermore, these nanoparticles commonly exhibit shortcomings such as poor thermal stability, inadequate tissue delivery, low delivery efficiency, short circulation time, and a tendency to escape from blood vessels.

3.4 Gold Nano-star
Gold nano-stars (Au-NSs) are a type of gold nanoparticles characterized by their unique star-shaped morphology, which gives them distinct optical absorption at 830 nm and surface-enhanced Raman scattering (SERS) properties (Figure 5b). Au-NSs exhibit highly enhanced scattering and absorption properties compared to spherical nanoparticles due to their branched morphology and sharp tips leading to enhanced electromagnetic fields at the surface and leading to localized surface plasmon resonance [68] in the visible to near-infrared range, resulting in strong absorption and scattering of light [68], which enhances their SERS [69] activity. Au-NSs have a high surface area due to their branched structure, making them highly effective for applications such as optical sensing and biomedical imaging. This feature allows them to efficiently scatter and absorb light, enhancing the contrast and sensitivity of OCT imaging. Additionally, the plasmon resonance of gold nano-stars can be precisely tuned by adjusting their size and shape [70], enabling optimization for specific OCT imaging wavelengths. Furthermore, their multifunctional nature permits multimodal imaging when combined with other imaging modalities, such as photoacoustic or fluorescence imaging, offering complementary information for improved tissue characterization [71]. Au-NSs are typically synthesized through seed-mediated growth methods, where gold seeds are grown anisotropically in the presence of a reducing agent and a shape-directing agent [72]. Silver ions are often used as catalysts to induce the growth of branched structures during synthesis [73].

Therefore, Au-NSs also have several advantages for OCT due to their unique optical properties, making them promising contrast agents. Some benefits include enhanced scattering and absorption properties, tunable plasmon resonance, enhancing the contrast and sensitivity of OCT imaging, and the potential for multimodal imaging.

3.5 Gold Nano-rod
Gold nanorods (Au-NRs) are nanoscale structures composed of gold atoms arranged in a rod-like shape rod-shaped nanoparticle with unique optical properties [74]. They exhibit unique optical properties due to their aspect ratio

and surface plasmon resonance [74]. Typically, the UV-vis peaks are at 800-900 nm, depending on the particle size (Figure 5c). Au-NRs have tunable optical properties. The optical absorption peak of gold nanorods can be tuned across the visible to near-infrared (IR) spectrum by adjusting their aspect ratio [74]. Moreover, gold nanorods exhibit a high surface area-to-volume ratio. This property makes them suitable for various applications in catalysis, sensing, imaging, and therapeutics. Au-NRs have biocompatibility properties, and they are often functionalized to enhance their biocompatibility for biomedical applications [74].

The Au-NRs can be prepared using the seed-mediated growth method. A method involving the reduction of gold salts in the presence of surfactants and seeds to control the aspect ratio of nanorods [74]. Moreover, Au-NRs were fabricated using template-assisted methods, such as porous membranes, to guide the growth of nanorods [74].
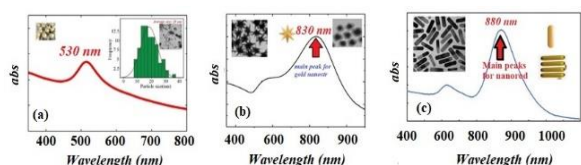

Figure 5. UV-vis Spectrum and particle shape of a) Au-NPs, b) Au-NSs, and c) Au-NRs.

Gold nanostructures (Au-NPs, Au-NSs, and Au-NRs) exhibit remarkable light absorption and scattering capabilities due to their efficient interaction with light. This interaction is attributed to the collective oscillation of conduction electrons on the nanoparticle's surface when illuminated with specific wavelengths, known as surface plasmon resonance (SPR). This phenomenon significantly enhances absorption and scattering intensities compared to nanoparticles lacking this property. Moreover, the absorption and scattering properties of gold structures can be finely adjusted by manipulating factors such as particle size, shape, and the local refractive index surrounding the particle surface.

The optical properties of Au-NRs exhibit unique optical properties primarily due to their LSPR phenomenon [75]. The frequency of LSPR depends on the size, shape, and dielectric environment of the nanorods [76]. Moreover, the optical properties of Au-NRs, including absorption and scattering spectra, can be tuned by adjusting parameters such as aspect ratio, size, and surface chemistry [75]. By changing the aspect ratio of nanorods, their optical absorption peak can be shifted across the visible and near-infrared spectrum [76]. Therefore, Au-NRs find applications in various fields such as biomedical imaging, photothermal therapy, sensing, and catalysis due to their tunable optical properties [76]. Au-NRs exhibit strong optical scattering and absorption properties in the near-infrared (NIR) region, which matches well with the imaging window of OCT. This property allows Au-NRs to serve as efficient contrast agents, enhancing the contrast and sensitivity of OCT imaging. Moreover, their tunable aspect ratio and surface chemistry enable precise control over optical properties and functionalization, facilitating molecular targeting for specific imaging applications in biological tissues [29].

3.6 Copper Sulfide Nanoparticles

Copper sulfide nanoparticles (CuS-NPs) have garnered attention due to their various applications in fields like electronics, catalysis, and biomedicine. CuS-NPs are nanoscale particles composed of copper and sulfur atoms. They exhibit unique optical, electrical, and catalytic properties due to their small size and high surface area [77]. CuS-NPs show interesting optical properties that can be utilized in optoelectronic devices and sensors [77]. The crystalline properties of CuS NPs affect their behavior and performance in various applications [77]. CuS-NPs can be prepared using chemical and colloidal methods. Chemical Precipitation involves the chemical reaction between copper and sulfur precursors in a suitable solvent under controlled conditions to form CuS nanoparticles [77]. CuS-NPs can be prepared using a two-phase colloidal synthesis method, where the Cu:S ratio can be adjusted to control the properties of the resulting nanoparticles [78]. CuS-NPs exhibit absorption in the visible and near-infrared regions of the electromagnetic spectrum [79]. The absorption characteristics can be tailored by controlling the size, shape, and crystalline structure of the nanoparticles [80]. The optical band gap of CuS-NPs influences their optical behavior, such as light absorption and emission [81]. This band

gap energy can be determined through techniques like UV-Vis and photoluminescence spectroscopy [81]. CuS-NPs have been explored for various biological applications due to their unique optical properties, including imaging and photothermal therapy [79]. CuS-NPs as a p-type semiconductor, possesses optical characteristics superior to materials like gold and silver, making it attractive for certain optoelectronic and bioimage applications [79]. CuS-NPs have shown potential benefits for OCT due to their mentioned optical and physical properties. One significant advantage is their ability to enhance the contrast and sensitivity of OCT imaging, particularly in biological tissue imaging [80]. Therefore, CuS-NPs offer improved contrast and sensitivity in OCT imaging due to their strong optical scattering properties [80]. When used as contrast agents, these nanoparticles can enhance the visualization of tissue structures and pathological features, leading to better diagnostic accuracy. Additionally, CuS-NPs have been explored for their potential as theranostic agents, allowing for simultaneous imaging and therapeutic intervention in biomedical applications [32, 81].

3.7 Quantum dots
Quantum dots (QDs) are nanoscale semiconductor particles that exhibit unique optical and electronic properties due to quantum confinement effects. The main properties of QDs are size-tunable emission, high quantum yield, narrow emission band, photostability, and broad absorption. They typically have sizes ranging from 2 to 10 nanometers. QDs are composed of semiconductor materials such as cadmium selenide (CdSe), cadmium sulfide (CdS), indium arsenide (InAs), or lead sulfide (PbS) [82]. The emission wavelength of QDs can be precisely tuned by controlling their size, leading to a broad range of colors. QDs exhibit high quantum yield, meaning they efficiently emit light upon excitation. They possess narrow emission spectra, resulting in vibrant and pure colors. QDs are resistant to photobleaching, making them suitable for long-term imaging applications. QDs can absorb a wide range of wavelengths, enabling excitation with a single light source [83]. There are several methods for preparing QDs, including colloidal synthesis, organic synthesis, ligand exchange, and layer-by-layer assembly. QDs are commonly synthesized via colloidal methods, involving the reaction of precursor compounds in a solvent at high temperature in the presence of stabilizing ligands. Organic synthesis methods are also used, where precursors are reacted under controlled conditions, often in the presence of organic ligands. Following synthesis, ligand exchange techniques are employed to replace original ligands on the QD surface with more functional ligands for specific applications. QDs can be incorporated into thin films or multilayer structures using layer-by-layer assembly techniques, facilitating the fabrication of advanced electronic and optoelectronic devices [84].

QDs offer several benefits for OCT, a non-invasive imaging technique widely used in medical diagnostics, particularly in ophthalmology. Some of the advantages of QDs for OCT are as follows:

a) Improved Contrast and Sensitivity:
QDs have high quantum efficiency and narrow emission spectra, allowing for enhanced contrast and sensitivity in OCT imaging. This enables better visualization of tissue structures and pathological features, leading to improved diagnostic accuracy [85].

b) Multimodal Imaging Capabilities:
QDs can be functionalized to target specific biomolecules or cellular structures, enabling multimodal imaging when combined with other contrast agents or imaging modalities. This integration enhances the capabilities of OCT by providing complementary information, such as molecular or cellular-level details, which can aid in disease detection and monitoring [86].

c) Long-Term Stability and Biocompatibility:
QDs exhibit excellent photostability, resisting photobleaching and degradation over time. Additionally, they can be engineered to be biocompatible, minimizing potential cytotoxicity and ensuring long-term viability for in vivo imaging applications. These properties make quantum dots suitable for longitudinal studies and longitudinal monitoring of disease progression [87].

d) Depth-Resolved Imaging:
OCT relies on measuring backscattered light to generate cross-sectional images of tissues with micrometer-scale resolution. QDs, with their tunable emission wavelengths, can be used as contrast agents to enhance the signal-to-noise ratio of OCT images, facilitating depth-resolved

imaging of tissue structures, such as retinal layers or tumor margins [87].

e) Targeted Molecular Imaging:

Functionalized quantum dots can target specific molecular markers associated with diseases, such as cancer biomarkers or inflammatory molecules. By conjugating targeting ligands to QDs, OCT can achieve molecular-specific imaging, allowing for early detection, precise localization, and characterization of pathological tissues [85, 87].

Consequently, quantum dots offer several advantages for enhancing the capabilities of optical coherence tomography, including improved contrast and sensitivity, multimodal imaging capabilities, long-term stability, depth-resolved imaging, and targeted molecular imaging. These benefits make quantum dots promising contrast agents for advancing OCT imaging in various biomedical applications, particularly in ophthalmology, oncology, and neurology.

4. Delivery Methods to use plasmonic nanoparticles for OCT

When the lateral resolution is calculated with the diameter of the probe beam, the depth resolution of OCT depends on the source coherence length, and it is in the range of 6 to 15 μm in air. Nano-sensitive OCT image is an innovative design that offers increased sensitivity to nanometer-scale structural changes or measurements [88-91]. Despite the difficulty in depicting cellular or sub-cellular level structures, OCT's imaging resolution is at least 20 times superior to other in vivo 3D imaging techniques like ultrasound. Interferometry ensures that OCT selectively measures only the backscattered light directly from the surfaces of interest in tissue while rejecting most photons that scatter multiple times or come from other incoherent light sources. This is crucial for producing clear, high-resolution 3D images of thick samples with minimal background noise. Still, it also limits OCT from easily leveraging molecular processes such as bioluminescence emission, fluorescence emission, and Raman scattering. Essentially, OCT images represent the intensity of backscattered probe light, which is influenced by variations in the refractive index of a sample. Unfortunately, distinguishing between most bio-molecular species based solely on their refractive indexes is challenging, making the development of molecular contrast OCT systems a complex task. Briefly, the nanoparticles and the plasmonic properties of metal nanoparticles effectively improve the OCT image. Therefore, plasmonic nanoparticles can be used as a contrast agent in OCT to enhance the imaging capabilities and qualities by increasing the contrast and specificity of the images. Nanomaterials provide better diagnostic capabilities in the OCT system. These agents as molecular contrast agents are designed to bind to specific molecular targets within the tissue, enhancing the OCT signal at those locations. This enables more detailed imaging of specific cellular or molecular structures [92]. The agents can be used in a dynamic and integration regime. The Dynamics regime utilizes fluctuations in OCT signals caused by contrast agents to enhance image contrast. It improves the visualization of dynamic processes and tissue microstructures [93]. Determining the refractive index and scattering properties of contrast agents is crucial. Techniques based on OCT are used to characterize these optical properties, ensuring the agents provide the desired contrast enhancement [94]. Different contrast agents, such as gold nanoparticles, dyes, and microbubbles, are evaluated for their effectiveness in enhancing OCT images. Their biocompatibility and specificity for targeting certain tissues are key factors in their selection [95]. Integration OCT Systems is a particular form. The spatial information regarding the concentration and displacement of contrast agents can be determined by integrating them with OCT systems. This integration allows for real-time imaging and monitoring of the distribution and effect of the contrast agents within the tissue. Consequently, by using these approaches, OCT imaging is significantly improved, allowing for more precise and detailed visualization of biological tissues.

The main steps to experiment are the selection of nanomaterials [96] and functionalization with bioconjugates, and ligands to target specific tissues or cellular markers [97] to consider the experimental method for plasmonic OCT. They can significantly improve the capabilities of OCT, making it a more powerful tool for medical diagnostics and research. The importance of

nanoparticle selection and functionalization with bioconjugates is the enhancement of scattering light and the contract images [97], respectively. They improve contrast by modulating the intensity of backscattered light. This is achieved through their high reflectance and scattering properties, which enhance the OCT signal and provide clearer images [98]. Nanomaterials can be used in dynamic contrast OCT (DyC-OCT) to capture fluctuations in the OCT signal, and in molecular contrast OCT to highlight specific molecular targets within the tissue [99].

Using nanomaterials as contrast agents in OCT involves either injection or topical application methods, such as drop liquids.

4.1. Injection Method
The first method for injection of nanomaterial is intravenous Injection. Nanoparticles are suspended in a biocompatible solution and injected into the bloodstream. This allows the nanoparticles to circulate and target specific tissues or organs for enhanced OCT imaging [99].The second method for using the nanoparticles in OCT experiments is direct tissue injection. For localized imaging, nanoparticles can be directly injected into the tissue of interest. This method ensures a higher concentration of nanoparticles in the targeted area, providing better contrast [96].

4.2 Drop liquid (Topical Application)
The drop method can be utilized in two regimes as follows:

Topical Drops: Nanoparticles can be delivered as drops on the tissue surface, such as the cornea or skin. This method is non-invasive and suitable for areas accessible from the surface. The nanoparticles penetrate the tissue and enhance OCT imaging [97].

Absorption and Penetration: The efficacy of this method depends on the nanoparticles' ability to penetrate the tissue layers and their retention at the target site.

The injection and drop methods (Figure 6) aim to enhance the contrast of OCT images by increasing the backscattered light beam, allowing for improved visualization of the tissue structures and potential abnormalities.

Wei et. al. reported the OCT imaging system based on a Gelatin/TiO2/India ink phantom [100]. Gelatin-based formulations can adjust optical properties easily with TiO2 and ink, unlike intralipid suspensions. A gelatin phantom with μa of 0.6 cm-1 and μs of 12.5 cm-1 was made. Images with noisy long frequencies formed a 2mm thick layer in containers.
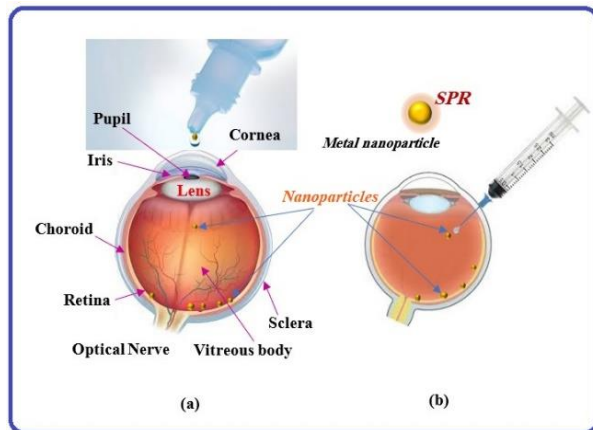

Figure 6. a) Anatomy of the eye and drop of the nanomedicine, b) Injection of nanomedicine in the eye.

5. Application of OCT (Eye, Skin, Dental)

The OCT with nanoparticles has more application in ophthalmology, dermatology, and gastrointestinology to diagnose the disease. Moreover, OCT can be used to obtain the image pattern of tooth layers in dentistry. In this section, the samples of OCT images have been presented for retina pattern, tooth pattern, and skin pattern.

5.1. Oct pattern of retina
Figure 7 shows the OCT standard image for the retina layer. The image shows the Nerve Fiber Layer (NFL), Ganglion Cell Layer (GCL), Inner Nuclear layer (INL), Outer Plexiform layer (OPL), Outer Nuclear Layer (ONL), External Limiting Membrane (ELM), Inner segment / outer segment layer (IS/OS), and Retinal Pigment Epithelium (RPE). The image was obtained using interaction of Ti:Al2O3 femtosecond laser with retina in the OCT setup based on Fourier domain configuration [54].
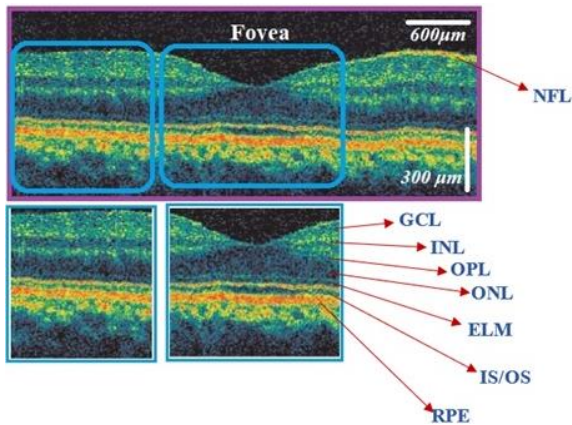
Figure 7. OCT standard image for demonstration of eight retina layers.

The role of nanoparticles and plasmonic metal nanoparticles is enhancement of resolution and contrast. As a literature, the experiments of each research have been carried out with mouse and other laboratory pets. Figure 8 shows the image of choroidal neovascularization (CN). Figures 8a and 8b demonstrate the CN in the normal case and CN when the Au-NPs were injected into the eyes [101]. As a result, the Au-NPs scattered the light, and the plasmonic wave exited in the CN area, so the CN can be seen clearly.
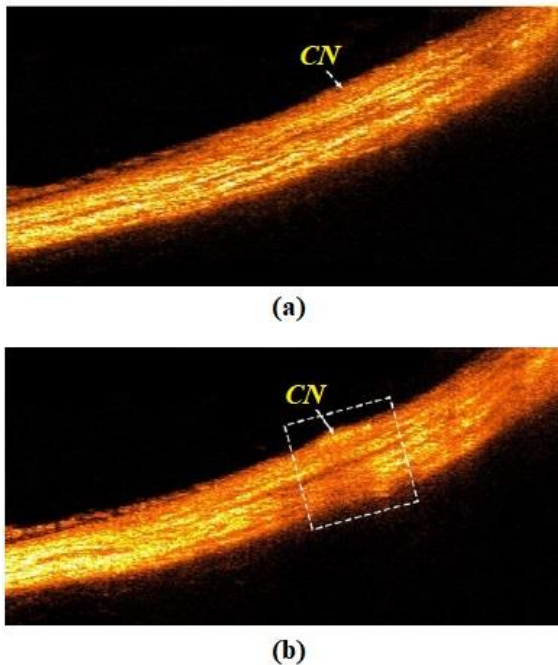

Figure 8. OCT image of choroidal neovascularization a) before injection of Au-NPs, b) after injection of Au-NPs.

5.2. OCT pattern of dentistry

One of the most common applications of OCT is in dentistry. This application is called OCT in nano-dentistry and it can be seen from two categories the OCT method works such as to make strides in the affectability or distinguish within the nanometer administration and the OCT procedure can be utilized to ponder nanostructures in dental materials or dental tissues (difficult or delicate).

Martin Leahy et al. [102] and J. Yi et al [103] work on nano-sensitive OCT (nsOCT) and reverse spectroscopic OCT (ISOCT), respectively. nsOCT utilizes micrometer resolution data from Fourier-domain OCT to achieve nanoscale imaging, while ISOCT evaluates the mass-density relationship by analyzing backscattering and scattering coefficients. These techniques have been utilized to assess wound healing in the cornea and detect structural changes in various tissues. The findings were validated through numerical simulations, tissue studies, and electron microscopy. Readers are encouraged to refer to the provided references for further details on these innovative imaging methods.

OCT is used to evaluate nanostructures within a test from the moment of application. In a pioneer application in nano-dentistry detailed in reference [104], gold nanoparticles (AuNP) were used as a contrasting agent for dental OCT by shaping them in situ. This advancement was crucial for imaging specific areas, such as the dentinal tubules as shown in Figure 9a. Initially, gold particles were dispersed in a dental bonding system and applied to the dentin, with the formation of AuNP during photopolymerization [104]. The diameter of the AuNP ranged from 40 to 120 nm, while dentinal tubule diameters ranged from 500 to 4000 nm. OCT images in Figure 9b demonstrate the effectiveness of AuNP in enhancing image clarity, with warm colors indicating higher scattering power. Without AuNP, images were unclear. The presence of AuNP made tubules easily distinguishable and enhanced OCT images, as shown by the arrows in Figure 6d. More details can be found in the reference [104].
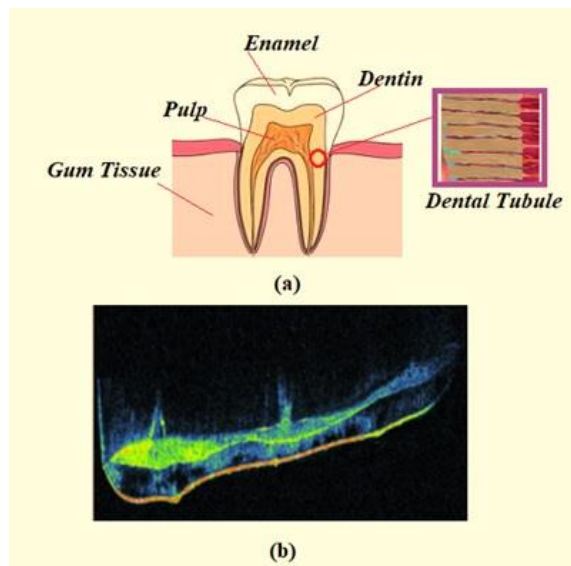
Figure 9. a) Tooth anatomy, b) OCT image.

Nano-dentistry has various applications, including the application of optical clearing agents (OCA) to improve optical coherence tomography for better diagnosis. Silver nanoparticles (Ag-NPs) are commonly used in nano-dentistry [105] due to their biocompatibility and antibacterial properties. The role of optical clearing agents in bio-tissue imaging is a dynamic area of research focused on enhancing imaging depth and overall healthcare outcomes. The physical process of optical clearing involves the use of biocompatible chemicals to enhance tissue permeability, refractive index matching, cellular dehydration, and collagen solubility. These agents have been used in various tissues, such as skin [96], bone, and cartilage, to improve imaging quality. In dentistry, OCA can help enhance the quality of OCT [96] imaging by facilitating deeper penetration and improving image contrast, especially in cases of caries lesions. Ag-NPs suspended in glycerol have been utilized as OCA for diagnosing early caries lesions through OCT imaging by enhancing birefringence changes in demineralized areas. Overall, OCA offers significant potential to improve imaging outcomes in dentistry and other medical fields by enhancing tissue visibility and image quality [96].

5.3. OCT pattern of skin

OCT is a non-invasive imaging technique that uses low-power infrared laser light to capture high-resolution images of skin tissues up to 2 mm deep. OCT has several key applications such as the diagnosis and monitoring of skin diseases, assessment of skin morphology, and guiding treatment in dermatology.

a) Diagnosis and Monitoring of Skin Diseases: OCT can help diagnose conditions like basal cell carcinoma, melanoma, and other skin lesions by providing detailed images of the skin layers and their structures. This allows for the monitoring of disease progression and treatment efficacy [106].

b) Assessment of Skin Morphology: The high-resolution cross-sectional and en-face images obtained from OCT can reveal changes in skin texture and morphology, aiding in the classification and study of various dermatological conditions [106].

c) Guiding Treatment: OCT can be used to guide surgical procedures by delineating tumor margins more precisely, reducing the risk of incomplete excision, and improving cosmetic outcomes [106].

The skin is a multi-layered (Figure 10(a), and 10(b)) structure ranging from 0.5-4mm thick. In OCT images, a thin hyporeflective line indicates the top layer of the skin [107]. Beneath this are the epidermis, dermal-epidermal junction, and dermis. OCT criteria in dermatological pathology include skin layer thickness [108], vascular organization, and structure. Studies using OCT have shown promise in evaluating various skin conditions. For example, SS-OCT was used to assess penile injuries, while DOCT was applied to acne lesions. OCT imaging has also been beneficial in diagnosing basal cell carcinoma and systemic sclerosis [109]. Additionally, OCT has shown potential in monitoring skin conditions and guiding treatment plans. Overall, OCT offers valuable insights into the skin's structure and can aid in the diagnosis and management of various dermatological conditions [109] including skin tumors, actinic keratosis in the skin (Figure 10 (b)), inflammatory skin diseases, skin cancer [110](Figure 10(e)), and checking the skin surface without any skin biopsy [111] to recognize the skin change. Utilizing ordinary

OCT, the stratum corneum of glabrous skin, the epidermis, and the upper dermis can be distinguished with a flat determination of 10-15 μm. Skin layers, blood vessels, and skin variations from the norm can be identified non-invasively. Headways in broadband light sources, like femtosecond Ti: sapphire laser, may before long permit ultra-high resolutions of around 1 μm, empowering cellular-level examination of skin tissue and potential separation between sound and hurtful tissues [106].

As mentioned above, plasmonic OCT is an advanced imaging technique that enhances traditional OCT using plasmonic nanoparticles, such as gold nanostars. This combination allows for improved contrast and specificity in skin imaging, making it particularly useful in dermatology. The plasmonic OCT enhanced imaging of skin microvasculature. Plasmonic OCT enables detailed visualization and differentiation of individual microvasculature, crucial for diagnosing and monitoring conditions such as skin cancer and other vascular-related skin diseases. The enhanced contrast provided by plasmonic nanoparticles makes it easier to detect abnormalities in the skin's blood vessels [101]. By combining plasmonic nanoparticles with OCT, clinicians can obtain detailed three-dimensional images of the skin at micron scales, offering a better understanding of the spatial organization of different skin layers and structures [112]. In addition, plasmonic OCT can provide molecular contrast, allowing for the identification of specific biomarkers within the skin. This capability is valuable in research and clinical settings for the early detection of skin diseases and monitoring treatment responses [99].
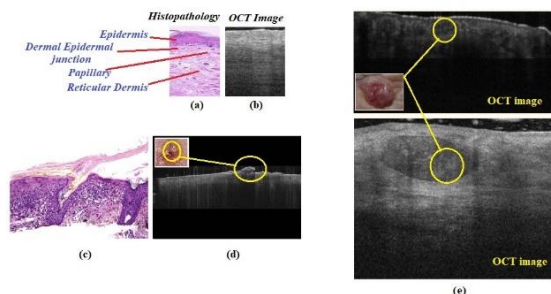
Figure 10. a) histopathology of normal skin, b) OCT pattern of normal skin, c) histopathology, d) OCT

image pattern of actinic keratosis of the skin, and e OCT image pattern of cancer in the skin.

6. Challenges and Future Outlook

OCT is a powerful imaging technique that provides high-resolution cross-sectional images of biological tissues. Enhancing OCT with nano particles such as gold nanoparticles, copper nanoparticles, CuS-NPs, carbon nanostructures (e.g., carbon nanotubes, graphene) and quantum dots holds great promise, particularly for biomedical applications like early cancer detection, tissue characterization, and drug delivery tracking. However, several challenges and considerations remain that have been shaped by ongoing research and technological advancements, including biocompatibility and toxicity, controlled delivery and targeting, optical properties tuning, instrumentation, signal interpretation, regulatory and manufacturing barriers. Moreover, multifunctional and hybrid nanoparticles, AI and image analysis, targeted and responsive nanoparticles, and improved optical design should be considered as the future outlook.

Conclusion

Optical coherence tomography is a non-invasive, powerful, and useful technique for image capture of the retina, monitoring of skin diseases, and nano-dentistry images. Time-domain and Fourier-domain techniques are the two main methods for analyzing and capturing OCT images. Coherence length, axial resolution, transverse resolution, depth range, and lateral field of view are significant parameters for evaluating and increasing the quality of OCT images. Therefore, the sensitivity, resolution, and speed of the system should be considered for enhancing and application of OCT devices based on the Michelson interferometer to capture biomedical images. The optical properties of nanostructures and the plasmonic properties of metal nanoparticles are the scientific approach to enhancing and improving the sensitivity, resolution, and response time of the OCT technique. Moreover, Au-NPs, Ag-NPs, Au-NSs, Au-NRs, CuS-NPs, and quantum dots are

known plasmonic and nanostructures for improving the quality of OCT images. nano-dentistry is the application of OCT based on nanostructure, and it has a more useful application for diagnosis in dentistry. The nanostructure enhances imaging contrast and disease detection, monitoring, and minimally invasive diagnostics in dentistry applications. Consequently, the application of plasmonic metal nanoparticles and nanostructures has improved and enhanced the image quality, response time, image contrast, biocompatible, and safety of OCT technique. In addition, the plasmonic nanostuctures enhanced the quality and significant parameters of the OCT.

References

1. Everett, M., et al., *Optical coherence tomography: From technology to applications in ophthalmology.* Translational Biophotonics, 2021. **3**(1): p. e202000012.
2. Bouma, B.E., et al., *Optical coherence tomography.* Nature Reviews Methods Primers, 2022. **2**(1): p. 79.
3. Fujimoto, J.G., et al., *Optical coherence tomography: an emerging technology for biomedical imaging and optical biopsy.* Neoplasia, 2000. **2**(1-2): p. 9-25.
4. Huang, D., et al., *Optical coherence tomography.* science, 1991. **254**(5035): p. 1178-1181.
5. Fercher, A.F., et al., *Optical coherence tomography-principles and applications.* Reports on progress in physics, 2003. **66**(2): p. 239.
6. Puliafito, C.A., et al., *Imaging of macular diseases with optical coherence tomography.* Ophthalmology, 1995. **102**(2): p. 217-229.
7. Tearney, G.J., et al., *Three-dimensional coronary artery microscopy by intracoronary optical frequency domain imaging.* JACC: Cardiovascular imaging, 2008. **1**(6): p. 752-761.
8. Drexler, W. and J.G. Fujimoto, *Optical coherence tomography: technology and applications*. 2008: Springer Science & Business Media.
9. Burns, S.A., et al., *Adaptive optics imaging of the human retina.* Progress in retinal and eye research, 2019. **68**: p. 1-30.
10. Choma, M.A., et al., *Sensitivity advantage of swept source and Fourier domain optical coherence tomography.* Optics express, 2003. **11**(18): p. 2183-2189.
11. Ogien, J., et al., *Dual-mode line-field confocal optical coherence tomography for ultrahigh-resolution vertical and horizontal section imaging of human skin in vivo.* Biomedical optics express, 2020. **11**(3): p. 1327-1335.
12. A. R. Sadrolhosseini, S.M.H.a.S.A., *Plasmonic Sensor for Detection of Biomolecular and Medical Diagnostics*, in *A Closer Look at Plasmonics*, C. Bosch, Editor. 2022. p. 1-55.
13. Nahas, A., et al., *Detection of plasmonic nanoparticles with full field-OCT: optical and photothermal detection.* Biomedical optics express, 2014. **5**(10): p. 3541-3546.
14. Wang, D., et al., *Recent Advances in Surface Plasmon Resonance Imaging Sensors.* Sensors, 2019. **19**(6): p. 1266.
15. Sherry, L.J., et al., *Localized surface plasmon resonance spectroscopy of single silver triangular nanoprisms.* Nano letters, 2006. **6**(9): p. 2060-2065.
16. Sadrolhosseini, A.R., S.M. Hamidi, and Y. Mazhdi, *Detection of gentamicin in water and milk using chitosan-ZnS-Au nanocomposite based on surface plasmon resonance imaging sensor.* Measurement, 2024: p. 115412.
17. Lal, S., S. Link, and N.J. Halas, *Nano-optics from sensing to waveguiding.* Nature photonics, 2007. **1**(11): p. 641-648.
18. Karathanasis, E., et al., *Imaging nanoprobe for prediction of outcome of nanoparticle chemotherapy by using mammography.* Radiology, 2009. **250**(2): p. 398-406.
19. Camden, J.P., D.J. Masiello, and B. Ren, *Spectroscopy and microscopy of plasmonic systems.* The Journal of Chemical Physics, 2021. **155**(9).
20. Lewis, D.Y., et al., *[18F] fluoroethyltyrosine-induced cerenkov luminescence improves image-guided*

surgical resection of glioma. Theranostics, 2018. **8**(14): p. 3991.

21. Wang, H., et al., *In vitro and in vivo two-photon luminescence imaging of single gold nanorods.* Proceedings of the National Academy of Sciences, 2005. **102**(44): p. 15752-15756.

22. Ghahrizjani, R.T., et al., *Highly sensitive H2S gas sensor containing simultaneously UV treated and self-heated Ag-SnO2 nanoparticles.* Sensors and Actuators B: Chemical, 2023. **391**: p. 134045.

23. Sharifi Malvajerdi, S., et al., *HVHC-ESD-Induced Oxygen Vacancies: An Insight into the Phenomena of Interfacial Interactions of Nanostructure Oxygen Vacancy Sites with Oxygen Ion-Containing Organic Compounds.* ACS Applied Materials & Interfaces, 2023. **15**(41): p. 48785-48799.

24. Ghahrizjani, R.T., et al., *ZnO–SrAl2O4: Eu nanocomposite-based optical sensors for luminescence thermometry.* ACS Applied Nano Materials, 2021. **4**(9): p. 9190-9199.

25. Hamidi, S.M., et al., *Plasmonic grating H 2 S sensor based on a chitosan-polyaniline-nano-composite.* Optical Materials Express, 2023. **13**(6): p. 1765-1779.

26. Sharifi Malvajerdi, S., et al., *High-voltage, high-current electrical switching discharge synthesis of ZnO nanorods: A new method toward rapid and highly tunable synthesis of oxide semiconductors in open air and water for optoelectronic applications.* ACS Applied Materials & Interfaces, 2021. **13**(39): p. 46951-46966.

27. Ahn, S., S.Y. Jung, and S.J. Lee, *Gold nanoparticle contrast agents in advanced X-ray imaging technologies.* Molecules, 2013. **18**(5): p. 5858-5890.

28. Li, J., et al., *Intravascular imaging of atherosclerosis by using engineered nanoparticles.* Biosensors, 2023. **13**(3): p. 319.

29. Kavalaraki, A., et al., *Gold nanoparticles as contrast agents in ophthalmic imaging.* Optics, 2023. **4**(1): p. 74-99.

30. de la Zerda, A., et al., *Optical coherence contrast imaging using gold nanorods in living mice eyes.* Clinical & experimental ophthalmology, 2015. **43**(4): p. 358-366.

31. Jiang, X., et al., *Controllably tuning the near-infrared plasmonic modes of gold nanoplates for enhanced optical coherence imaging and photothermal therapy.* RSC advances, 2015. **5**(98): p. 80709-80718.

32. Marin, R., et al., *Plasmonic copper sulfide nanoparticles enable dark contrast in optical coherence tomography.* Advanced Healthcare Materials, 2020. **9**(5): p. 1901627.

33. Hong, G., et al., *Carbon nanomaterials for biological imaging and nanomedicinal therapy.* Chemical reviews, 2015. **115**(19): p. 10816-10906.

34. Bakalova, R., et al., *Quantum dot-based western blot technology for ultrasensitive detection of tracer proteins.* Journal of the American Chemical Society, 2005. **127**(26): p. 9328-9329.

35. Aumann, S., et al., *Optical coherence tomography (OCT): principle and technical realization.* High resolution imaging in microscopy and ophthalmology: new frontiers in biomedical optics, 2019: p. 59-85.

36. Bille, J.F., *High resolution imaging in microscopy and ophthalmology: new frontiers in biomedical optics.* 2019.

37. Zhang, J., et al., *Time-domain full-field optical coherence tomography (TD-FF-OCT) in ophthalmic imaging.* Therapeutic Advances in Chronic Disease, 2023. **14**: p. 20406223231170146.

38. Fercher, A., K. Mengedoht, and W. Werner, *Eye-length measurement by interferometry with partially coherent light.* Optics letters, 1988. **13**(3): p. 186-188.

39. Wang, L.V. and H.-i. Wu, *Biomedical optics: principles and imaging.* 2007: John Wiley & Sons.

40. Bousi, E., I. Charalambous, and C. Pitris, *Optical coherence tomography axial resolution improvement by step-frequency encoding.* Optics Express, 2010. **18**(11): p. 11877-11890.

41. Burkhardt, A., et al., *Endoscopic optical coherence tomography device for forward imaging with broad field of view.* Journal of biomedical optics, 2012. **17**(7): p. 071302-071302-5.

42. Bouma, B.E., et al., *Fourier-domain optical coherence tomography: recent advances*

toward clinical utility. Current opinion in biotechnology, 2009. **20**(1): p. 111-118.

43. De Boer, J.F., R. Leitgeb, and M. Wojtkowski, *Twenty-five years of optical coherence tomography: the paradigm shift in sensitivity and speed provided by Fourier domain OCT.* Biomedical optics express, 2017. **8**(7): p. 3248-3280.

44. Leitgeb, R., et al., *Ultrahigh resolution Fourier domain optical coherence tomography.* Optics express, 2004. **12**(10): p. 2156-2165.

45. Kalkman, J., *Fourier-Domain Optical Coherence Tomography Signal Analysis and Numerical Modeling.* International Journal of Optics, 2017. **2017**(1): p. 9586067.

46. Samavati, K., M. Taghi Tavassoly, and H. Ghomi, *Representation of image distortion by Moiré fringes at phase singularity state.* Applied Optics, 2017. **56**(2): p. 324-329.

47. Tavassoly, M.T. and K. Samavati, *Formulation of the moiré fringes formed by superimposing linear gratings with slowly varying parameters.* Applied Optics, 2014. **53**(28): p. 6612-6618.

48. Liu, C.-C., et al. *The effects of Gaussian beams on optical coherence tomography.* in *European Conference on Biomedical Optics.* 2007. Optica Publishing Group.

49. Zeppieri, M., et al., *Optical Coherence Tomography (OCT): A Brief Look at the Uses and Technological Evolution of Ophthalmology.* Medicina, 2023. **59**(12): p. 2114.

50. Baskaran, K. and C. Wildsoet, *Optical Coherence Tomography (OCT): Newer technologies and technical challenges.* Scandinavian Journal of Optometry and Visual Science, 2022. **15**(1).

51. Welzel, J., *Optical coherence tomography in dermatology: a review.* Skin Research and Technology: Review article, 2001. **7**(1): p. 1-9.

52. Anvari, P., et al., *Artifacts in optical coherence tomography angiography.* Journal of Ophthalmic & Vision Research, 2021. **16**(2): p. 271.

53. Montuoro, A., et al. *Motion artefact correction in retinal optical coherence tomography using local symmetry.* in *Medical Image Computing and Computer-Assisted Intervention–MICCAI 2014: 17th International Conference, Boston, MA, USA, September 14-18, 2014, Proceedings, Part II 17.* 2014. Springer.

54. Drexler, W., et al., *Ultrahigh-resolution ophthalmic optical coherence tomography.* Nature medicine, 2001. **7**(4): p. 502-507.

55. Zheng, S., et al., *Optical coherence tomography for three-dimensional imaging in the biomedical field: a review.* Frontiers in Physics, 2021. **9**: p. 744346.

56. Ahlers, C., et al., *Imaging of the retinal pigment epithelium in age-related macular degeneration using polarization-sensitive optical coherence tomography.* Investigative ophthalmology & visual science, 2010. **51**(4): p. 2149-2157.

57. Brahme, A., *Comprehensive biomedical physics.* 2014: Newnes.

58. de Carvalho, E.R. and P.M. Maloca, *Overview of optical coherence tomography in neuro-ophthalmology.* Annals of Eye Science, 2020. **5**: p. 14-14.

59. Pacholski, C., et al., *Plasmonic biosensors fabricated by galvanic displacement reactions for monitoring biomolecular interactions in real time.* Analytical and Bioanalytical Chemistry, 2020. **412**: p. 3433-3445.

60. Kim, K.Y., *Plasmonics: principles and applications.* 2012: BoD–Books on Demand.

61. Schasfoort, R.B., *Handbook of surface plasmon resonance.* 2017: Royal Society of Chemistry.

62. Yu, L.-B., et al., *Physical origin of directional beaming emitted from a subwavelength slit.* Physical Review B—Condensed Matter and Materials Physics, 2005. **71**(4): p. 041405.

63. Abdulhalim, I., *Coupling configurations between extended surface electromagnetic waves and localized surface plasmons for ultrahigh field enhancement.* Nanophotonics, 2018. **7**(12): p. 1891-1916.

64. Liu, N., et al., *Nanoantenna-enhanced gas sensing in a single tailored nanofocus.* Nature materials, 2011. **10**(8): p. 631-636.

65. Sevieri, M., et al., *Indocyanine green nanoparticles: are they compelling for cancer treatment?* Frontiers in chemistry, 2020. **8**: p. 535.

66. Huang, X., et al., *Cancer cell imaging and photothermal therapy in the near-infrared region by using gold nanorods.* Journal of the American Chemical Society, 2006. **128**(6): p. 2115-2120.

67. Lee, T.M., et al., *Engineered microsphere contrast agents for optical coherence tomography.* Optics letters, 2003. **28**(17): p. 1546-1548.

68. Nehl, C.L., H. Liao, and J.H. Hafner, *Optical properties of star-shaped gold nanoparticles.* Nano letters, 2006. **6**(4): p. 683-688.

69. Becerril-Castro, I.B., et al., *Gold nanostars: Synthesis, optical and SERS analytical properties.* Analysis & Sensing, 2022. **2**(3): p. e202200005.

70. Tsoulos, T., et al., *A closer look at the physical and optical properties of gold nanostars: an experimental and computational study.* Nanoscale, 2017. **9**(11): p. 3766-3773.

71. Yuan, H., et al., *Gold nanostars: surfactant-free synthesis, 3D modelling, and two-photon photoluminescence imaging.* Nanotechnology, 2012. **23**(7): p. 075102.

72. Minati, L., et al., *One-step synthesis of star-shaped gold nanoparticles.* Colloids and Surfaces A: Physicochemical and Engineering Aspects, 2014. **441**: p. 623-628.

73. Sahoo, G.P., et al., *Synthesis and photo physical properties of star shaped gold nanoparticles.* Colloids and Surfaces A: Physicochemical and Engineering Aspects, 2011. **375**(1-3): p. 30-34.

74. Khan, N.U., et al., *Synthesis of gold nanorods and their performance in the field of cancer cell imaging and photothermal therapy.* Cancer Nanotechnology, 2021. **12**: p. 1-33.

75. Park, K., et al., *Engineering the optical properties of gold nanorods: independent tuning of surface plasmon energy, extinction coefficient, and scattering cross section.* The Journal of Physical Chemistry C, 2014. **118**(11): p. 5918-5926.

76. Huang, X. and M.A. El-Sayed, *Gold nanoparticles: Optical properties and implementations in cancer diagnosis and photothermal therapy.* Journal of advanced research, 2010. **1**(1): p. 13-28.

77. Goswami, N., *Crystalline properties and optical processes in copper sulphide nanoparticles synthesized by chemical precipitation method.* Materials Today: Proceedings, 2023.

78. Al-Jawad, S.M., A.A. Taha, and M.M. Muhsen. *Preparation and characterization of CuS nanoparticles prepared by two-phase colloidal method.* in *Journal of Physics: Conference Series.* 2021. IOP Publishing.

79. ul Ain, N., et al., *Copper sulfide nanostructures: synthesis and biological applications.* RSC advances, 2022. **12**(12): p. 7550-7567.

80. Riyaz, S., A. Parveen, and A. Azam, *Microstructural and optical properties of CuS nanoparticles prepared by sol–gel route.* Perspectives in Science, 2016. **8**: p. 632-635.

81. Achimovičová, M., et al., *Structural and optical properties of nanostructured copper sulfide semiconductor synthesized in an industrial mill.* Frontiers of Chemical Science and Engineering, 2019. **13**: p. 164-170.

82. Hollingsworth, J.A. and V.I. Klimov, *1 "Soft" Chemical.* Nanocrystal Quantum Dots, 2010: p. 1.

83. Reiss, P., M. Protiere, and L. Li, *Core/shell semiconductor nanocrystals.* small, 2009. **5**(2): p. 154-168.

84. Qu, L. and X. Peng, *Control of photoluminescence properties of CdSe nanocrystals in growth.* Journal of the American Chemical Society, 2002. **124**(9): p. 2049-2055.

85. Sarwat, S., et al., *Quantum dots in ophthalmology: a literature review.* Current Eye Research, 2019. **44**(10): p. 1037-1046.

86. Ma, Y., et al., *Nanomaterials in the diagnosis and treatment of ophthalmic diseases.* Nano Today, 2024. **54**: p. 102117.

87. Zheng, Z. and Q. Xia, *Enhancement of Optical Coherence Tomography for Early Diagnostics Through Ag-Decorated ZnO Quantum Dots-Induced Motion Analysis.* Journal of Nanoelectronics and Optoelectronics, 2023. **18**(12): p. 1451-1457.

88. Duffy, N., et al., *In vitro detection of structural changes in chondrogenic mesenchymal stem cell pellets at the nano-scale using nano-sensitive optical coherance tomography.* Osteoarthritis and Cartilage, 2021. **29**: p. S24-S25.

89. Lal, C., et al., *Nanosensitive optical coherence tomography to assess wound healing within the cornea.* Biomedical Optics Express, 2020. **11**(7): p. 3407-3422.

90. Dsouza, R., et al., *In vivo detection of nanometer-scale structural changes of the human tympanic membrane in otitis media.* Scientific reports, 2018. **8**(1): p. 8777.

91. Das, N., et al., *Characterization of nanosensitive multifractality in submicron scale tissue morphology and its alteration in tumor progression.* Journal of biomedical optics, 2021. **26**(1): p. 016003-016003.

92. Yang, C., *Molecular Contrast Optical Coherence Tomography: A Review¶.* Photochemistry and Photobiology, 2005. **81**(2): p. 215-237.

93. Ren, C., et al., *Dynamic contrast optical coherence tomography (DyC-OCT) for label-free live cell imaging.* Communications Biology, 2024. **7**(1): p. 278.

94. Lee, T.-M., et al. *Optical characterization of contrast agents for optical coherence tomography.* in *Genetically Engineered and Optical Probes for Biomedical Applications*. 2003. SPIE.

95. Ehlers, J.P., et al., *Evaluation of contrast agents for enhanced visualization in optical coherence tomography.* Investigative ophthalmology & visual science, 2010. **51**(12): p. 6614-6619.

96. Das, A., et al., *Exploiting nanomaterials for optical coherence tomography and photoacoustic imaging in nanodentistry.* Nanomaterials, 2022. **12**(3): p. 506.

97. Gabriele, M.L., *Nanoparticle contrast agents for optical coherence tomography.* 2010, University of Pittsburgh.

98. Mackiewicz, M.R. and S. Huo, *Nanomaterials with High Reflectance for use as Contrast Agents for Optical Coherence Tomography Imaging.* Investigative Ophthalmology & Visual Science, 2023. **64**(8): p. 4671-4671.

99. Wang, A., et al., *Molecular contrast optical coherence tomography and its applications in medicine.* International journal of molecular sciences, 2022. **23**(6): p. 3038.

100. Wei, M., et al. *Using Plasmon-resonant Gold Nanorods as Absorption Contrast Agents for Optical Coherence Tomography.* in *Asia Optical Fiber Communication and Optoelectronic Exposition and Conference*. 2008. Shanghai: Optica Publishing Group.

101. Nguyen, V.-P., et al., *Plasmonic Gold Nanostar-Enhanced Multimodal Photoacoustic Microscopy and Optical Coherence Tomography Molecular Imaging To Evaluate Choroidal Neovascularization.* ACS Sensors, 2020. **5**(10): p. 3070-3081.

102. Lal, C., et al., *Nanosensitive optical coherence tomography to assess wound healing within the cornea.* Biomed Opt Express, 2020. **11**(7): p. 3407-3422.

103. Yi, J., et al., *Can OCT be sensitive to nanoscale structural alterations in biological tissue?* Opt Express, 2013. **21**(7): p. 9043-59.

104. Braz, A.K., et al., *In situ gold nanoparticles formation: contrast agent for dental optical coherence tomography.* J Biomed Opt, 2012. **17**(6): p. 066003.

105. Teixeira, J.A., et al., *Effects of a New Nano-Silver Fluoride-Containing Dentifrice on Demineralization of Enamel and Streptococcus mutans Adhesion and Acidogenicity.* International journal of dentistry, 2018. **2018**(1): p. 1351925.

106. Gambichler, T., et al., *Applications of optical coherence tomography in dermatology.* Journal of dermatological science, 2005. **40**(2): p. 85-94.

107. Ulrich, M., et al., *Dynamic optical coherence tomography in dermatology.* Dermatology, 2016. **232**(3): p. 298-311.

108. Wessels, R., et al., *Optical coherence tomography accurately identifies patients with penile (pre) malignant lesions: a single center prospective study.* Urology Annals, 2015. **7**(4): p. 459-465.

109. Wang, Y., et al., *Application of optical coherence tomography in clinical diagnosis.* Journal of X-ray Science and Technology, 2019. **27**(6): p. 995-1006.

110. Forsea, A.-M., et al., *Clinical application of optical coherence tomography for the imaging of non–melanocytic cutaneous tumors: A pilot multi–modal study.* Journal of medicine and Life, 2010. **3**(4): p. 381.

111. Hamdoon, Z., et al., *Optical coherence tomography-guided photodynamic therapy for skin cancer: case study.* Photodiagnosis and Photodynamic Therapy, 2011. **8**(1): p. 49-52.

112. P Mattison, S., et al., *Molecular imaging in optical coherence tomography.* Current Molecular Imaging (Discontinued), 2014. **3**(2): p. 88-105.